Video Article

In vivo Imaging of Optic Nerve Fiber Integrity by Contrast-Enhanced MRI in Mice

Stefanie Fischer*[1], Christian Engelmann*[2], Karl-Heinz Herrmann[3], Jürgen R. Reichenbach[3], Otto W. Witte[1], Falk Weih[2], Alexandra Kretz[1], Ronny Haenold[2]

[1]Hans Berger Department of Neurology, Jena University Hospital

[2]Immunology, Leibniz Institute for Age Research, Fritz Lipmann Institute, Jena

[3]Institute of Diagnostic and Interventional Radiology, Medical Physics Group, Jena University Hospital

*These authors contributed equally

Correspondence to: Ronny Haenold at rhaenold@fli-leibniz.de

Abstract

The rodent visual system encompasses retinal ganglion cells and their axons that form the optic nerve to enter thalamic and midbrain centers, and postsynaptic projections to the visual cortex. Based on its distinct anatomical structure and convenient accessibility, it has become the favored structure for studies on neuronal survival, axonal regeneration, and synaptic plasticity. Recent advancements in MR imaging have enabled the *in vivo* visualization of the retino-tectal part of this projection using manganese mediated contrast enhancement (MEMRI). Here, we present a MEMRI protocol for illustration of the visual projection in mice, by which resolutions of $(200 \ \mu m)^3$ can be achieved using common 3 Tesla scanners. We demonstrate how intravitreal injection of a single dosage of 15 nmol $MnCl_2$ leads to a saturated enhancement of the intact projection within 24 hr. With exception of the retina, changes in signal intensity are independent of coincided visual stimulation or physiological aging. We further apply this technique to longitudinally monitor axonal degeneration in response to acute optic nerve injury, a paradigm by which Mn^{2+} transport completely arrests at the lesion site. Conversely, active Mn^{2+} transport is quantitatively proportionate to the viability, number, and electrical activity of axon fibers. For such an analysis, we exemplify Mn^{2+} transport kinetics along the visual path in a transgenic mouse model (NF-κB $p50^{KO}$) displaying spontaneous atrophy of sensory, including visual, projections. In these mice, MEMRI indicates reduced but not delayed Mn^{2+} transport as compared to wild type mice, thus revealing signs of structural and/or functional impairments by NF-κB mutations.

In summary, MEMRI conveniently bridges *in vivo* assays and *post mortem* histology for the characterization of nerve fiber integrity and activity. It is highly useful for longitudinal studies on axonal degeneration and regeneration, and investigations of mutant mice for genuine or inducible phenotypes.

Video Link

The video component of this article can be found at http://www.jove.com/video/51274/

Introduction

Based on its favorable neuro-anatomical structure the rodent visual system offers unique possibilities to evaluate pharmacological compounds and their capability to mediate neuroprotection[1] or pro-regenerative effects[2,3]. Moreover, it allows studies on the functional and neuro-anatomical characteristics of mouse mutants, as recently exemplified for mice lacking the presynaptic scaffolding protein Bassoon[4]. Furthermore, a broad spectrum of supplementary tools affords additional featuring of retinal ganglion cell (RGC) and RGC axon numbers as well as RGC activity, *e.g.*, by electroretinography and behavioral tests, and the determination of cortical rearrangements by optical imaging of intrinsic signals. The latest technical developments in laser microscopy enable the *in situ* visualization of RGC regeneration by deep tissue fluorescence imaging in whole mount specimens of optic nerve (ON) and brain. In this histological approach, tetrahydrofuran based tissue clearing in combination with light sheet fluorescence microscopy permits the resolution of single fibers that re-enter into the deafferented ON and optic tract [5]. While such techniques might be superior in resolution and determination of growth patterns, they do not enable repetitive and longitudinal analyses of individual growth events, which are particularly desired to assess the process of long term regeneration.

Contrast-enhanced MRI has been employed for the minimal invasive visualization of the retino-tectal projection in mice and rats[6,7]. This can be achieved by direct intraocular delivery of paramagnetic ions (*e.g.*, Mn^{2+}) to retinal cells. As a calcium analog, Mn^{2+} is incorporated into RGC somata via voltage-gated calcium channels and actively transported along the axonal cytoskeleton of the intact ON and optic tract. While it accumulates in brain nuclei of the visual projection, *i.e.* the lateral geniculate nucleus (LGN) and superior colliculus (SC), transsynaptic propagation into the primary visual cortex appears negligible[8,9], although it may occur[10,11]. Under MR sequencing, paramagnetic Mn^{2+} augments MR contrast mainly by shortening T_1 spin-lattice relaxation time[12]. Such Mn^{2+} enhanced MRI (MEMRI) has been successfully

applied in various neuro-anatomical and functional studies of rats, including the assessment of axonal regeneration and degeneration after ON injury[13,14], the precise anatomical mapping of the retino-tectal projection[15], as well as the determination of axonal transport characteristics after pharmacological treatment[16]. Recent refinements in the dosage, toxicity, and kinetics of neuronal Mn^{2+} uptake and transport, as well as improved MRI protocols have extended its application to studies on transgenic mice[9] using 3 Tesla scanners commonly used in clinical practice[17].

Here, we present a MEMRI protocol suitable for longitudinal *in vivo* imaging of the mouse retino-tectal projection and exemplify its applicability by assessing Mn^{2+} dependent signal enhancement under naïve and various neurodegeneration conditions. Our protocol places specific emphasis on MR data acquisition in a moderate 3 T magnetic field that is generally more accessible than dedicated animal scanners. In naïve mice, we illustrate how tract-specific signal intensity can be substantially and reproducibly become increased after intravitreal (*ivit*) Mn^{2+} application. Quantitatively, Mn^{2+} propagation along the visual projection occurs independently of the normal aging process (measured between 3 and 26 month old mice) and augmentation is refractory to visual stimulation and adaptation to darkness. In contrast, Mn^{2+} enrichment in thalamic and midbrain centers is diminished following acute ON crush injury[18] as well as in *nfkb1* knock-out mice (*p50^{KO}*) suffering from spontaneous apoptotic RGC death and ON degeneration[19]. Thus, in expansion to conventional histological analysis, longitudinal MEMRI analysis of individual animals enables profiling of unique kinetics of neurodegenerative processes. This should prove useful for studies on neuroprotection and axonal regeneration associated with pharmacological or genetic interventions.

Protocol

All animal interventions are performed in accordance with the *European Convention for Animal Care and Use of Laboratory Animals* and the *ARVO Statement for the Use of Animals in Ophthalmic and Vision Research*. All experiments are approved by the local ethics committee. The procedure of ON injury in mice is described elsewhere[9].

1. Intravitreal Manganese Injection

1. Perform the Mn^{2+} injection 24 hr prior to the MR scan with the help of an assistant. Anesthetize the animals by intraperitoneal injection of a 5% chloral hydrate solution (420-450 mg/kg body weight in sterile PBS). For additional topical anesthesia, apply one drop of liquid conjuncain (0.4% oxybuprocaine hydrochloride) to the cornea prior to eye puncture. To inject 15 nmol Mn^{2+} per eye prepare a 7.5 mM $MnCl_2$ solution, *e.g.*, by diluting 1 L of 1 M $MnCl_2$ stock solution in 132 L H_2O. Load 5 μl of the final solution into a 5 μl Hamilton syringe connected to a 34 G small hub removable needle (RN needle).
2. When starting with the right eye, position the mouse left-sided under a binocular microscope and gently open and fix the right eye between the thumb and forefinger of your left hand. Pick up the syringe with your right hand and take hold of the needle close to the tip. For atraumatic puncture of the eye bulb, carefully insert the needle into the vitreous body at the infero-temporal circumference approximately 1 mm distal to the limbus, thereby sparing scleral vessels.
3. Next, the assistant slowly applies the total volume of 2 μl while controlling the scale of the Hamilton syringe. During this procedure, monitor optimal needle placement under the microscope and avoid puncture of the lens or spilling of the liquid. Keep the needle statically inserted for an additional 30 sec, then withdraw it slowly to minimize liquid leakage from the injection site.
4. Throughout the procedure, special care should be taken to avoid pressure to the eye. Likewise, avoid harsh or numerous attempts to puncture the eye bulb. Since Mn^{2+} uptake into RGCs and transport along the ON is already saturated at 15 nmol $MnCl_2$, this minimizes signal variations by slightly imprecise injection volumes. For bilateral signal enhancement of the visual projection, repeat the injection procedure for the left eye.
5. Apply ofloxacin-containing (3 mg/ml) eye drops and panthenol-containing ointment once after the procedure to prevent ocular infections and drying of the eye. Return the mice to their cages under normal housing conditions until the start of the MR scan.

2. Animal Preparation for MRI

1. Anesthetize the mouse by administration of a 2%/98% isoflurane/oxygen gas mixture. Mount the mouse on a mouse holder in an almost horizontal, untwisted position. Insert it into the MR coil, which is then adjusted inside the MR scanner. Monitor respiration and heart rate by appropriate systems. For technical details, see Herrmann *et al*[20].
2. During MRI, supply anesthesia by continuous insufflation of an initially 1.5%/98.5% isoflurane/oxygen gas mixture via an evaporator connected to the mouse head holder by an integrated tube. During the scan, adjust the deepness of anesthesia according to the recorded vital parameters (*i.e.* aim for a stable respiration rate of about 40 breaths per minute). Using a heating device keep the body surface temperature stable between 35 and 37 °C, as measured by a thermal sensor positioned at the abdominal site of the mouse. For technical details, see Herrmann *et al*[17].
3. After the scan, liberate the mouse from the holder and supply with pure oxygen to accelerate recovery from anesthesia. Additionally, keep the body temperature stable by using a red light heating source.

3. MRI Protocol

1. The protocol is validated for a 3 Tesla scanner equipped with a dedicated, SNR-efficient, small animal coil (linearly polarized Litz coil) with an effective field of view of 35 mm × 38 mm diameter. Operate the coil in transmit-receive mode.
2. With the animal in its final position, adjust the tune and match of the coil with the aid of a frequency analyzer. Manually adjust the transmitter reference voltage and the shim currents to optimize image homogeneity and quality.
3. Acquire T_1 weighted 2D TSE images with a resolution of 0.5 mm × 0.5 mm × 2 mm in sagittal and transversal view for planning. Using the planning MR scans, acquire the MEMR images in coronal measurement direction, rotated to be parallel to the animal's head with phase encoding along the left-right direction. To minimize acquisition time, use a rectangular field of view adjusted to the actual head dimensions. Employ a spoiled 3D FLASH sequence (VIBE 3D) using the following parameters: base matrix 256, field of view 54 mm × 50.65 mm × 14.08

mm, using 93.8% rectangular field of view in phase encode direction, and 128 slices of 0.11-mm slice thickness with slice resolution set to 61%.
4. Activate the in-plane interpolation to create final images with 512 × 480 × 128, providing an effective resolution of 0.21 mm × 0.21 mm × 0.18 mm (0.1 mm × 0.1 mm × 0.09 mm interpolated), echo time T_E = 6.51 msec, repetition time T_R = 16 msec, bandwidth = 160 Hz/px, flip angle = 22°. Apply two averages and three repetitions to achieve a total acquisition time (T_A) of approximately 30 min.

4. MRI Data Analysis

1. Analyze the data using the software *syngo* fastView. For quantitative signal enhancement, select defined regions of interest in 2D planar MRI recordings and determine signal intensities (SI) of the enhanced structure (SI_{MEMRI}), tissue background (SI_{backgr}), and the standard deviation of the noise (SD_N). Where necessary, use a mouse brain atlas to facilitate neuro-anatomical orientation for LGN and SC structures. Calculate the contrast-to-noise ratio (CNR) using the formula:
2. $CNR = (SI_{MEMRI} - SI_{backgr}) / SD_N$
3. Quantify three consecutive images for mean CNR calculation for each sample. In bilaterally injected animals, analyze each hemisphere independently.
4. For depiction of horizontal, coronal and sagittal images, calculate multiplanar reconstructions from the original 3D MRI data set. These processed images are not recommended for quantitative analysis. To create animated 3D reconstructions (maximum intensity projections, MIPs) of the retino-tectal projection, use an angiography post-processing software module.

5. Mn^{2+} Autometallography (TIMM Staining)

1. For TIMM staining of Mn^{2+} traced brain structures following MEMRI, inject a dosage of 15-150 nmol Mn^{2+} *ivit* 24 hr prior to imaging.
2. After the MR scan, perfuse the animals with 30 ml ice-cold 0.325% Na_2S in PBS (pH 7.4). Dissect retinae and freeze samples in Frozen section.
3. Cut sequential, equatorial sections of 15 µm thickness on a cryotome.
4. Perform TIMM staining[21] in the absence of fixative and cryoprotection according to Angenstein *et al*[22].

6. Statistical Analysis

Perform statistical analyses using the Student's t-test for single comparisons, followed by post hoc ANOVA. Data are presented as mean ± standard error. Individual N numbers are given separately for each experiment. Results reaching $P ≤ 0.05$ are considered statistically significant ($P ≤ 0.05$, *; $P ≤ 0.01$, **; $P ≤ 0.001$, ***).

Representative Results

The ability of this imaging technique to accurately assess the vitality and functionality of the visual projection relies upon precise application of a nontoxic Mn^{2+} dosage to the vitreous body and its uptake by RGCs. This major assumption is tested in **Figure 1**, where layer specific Mn^{2+} uptake is demonstrated by autometallography (TIMM staining)[21]. Retina sections were analyzed at 24 hr after *ivit* application of either 15 nmol or 150 nmol Mn^{2+}, or PBS as control. At this time point, the Mn^{2+} injected retinae show maximum signal enhancement in T_1 weighted MRI (N = 3; dotted lines), whereas the PBS injected retina is not enhanced in signal (N = 3; dotted line) (**Figure 1**, left panel). Note the hyperintensive signal enhancement in the 150 nmol injected eye. In contrast, nonenhanced brain areas (asterisks) show similar background signal intensities for all conditions (green color). *Ivit* Mn^{2+} application increases overall TIMM staining particularly in the RGC layer and nerve fiber layer (NFL) (**Figure 1**, magnified insets in middle panel), which are confirmed by investigation of individual RGC somata following H & E co-labeling (right panel).

For *in vivo* imaging of the mouse retino-tectal projection, it is critical to select a special mouse MEMRI protocol where the operational parameters together with the equipment, as illustrated in **Figure 2**, are adapted to analyze mice in a 3 T field. Applying such a scanner setup, our earlier work revealed that for CNS image resolution a rat head coil is superior to a dedicated mouse whole body coil[17]. To fix the murine head and to properly adjust its position within the rat coil, we use a cradle and a conical tube with bite bar made of plastic, both of which are downscaled to meet the body dimensions of mice (**Figures 2A,B**). When images are acquired on a transversal T_1 weighted matrix implementing 3D gradient echo sequences, the generation of high-resolution images of (200 µm)^3 within 35 min of acquisition time can be expected. We strongly recommend the constant monitoring of vital functions during the scan. Adjustment of anesthesia together with postimaging oxygenation and body temperature control significantly accelerates recovery time and guarantees survival rates of about 100%. Such technical precautions are essential to ensure that the whole cohort will sustain longitudinal and repetitive MRI.

In any study, only a nontoxic Mn^{2+} dosage of 15 nmol should be used for *ivit* application[9], which is sufficient to prominently enhance CNRs in the retina, ON, and optic tract up to the presynaptic intracerebral LGN and SC. CNR values are best calculated from 200 µm thick transversal slices obtained from original MRI data sets by reslicing the original isotropic 3D volume. **Figure 3A** shows an example of precise CNR determination for the enhanced LGN, where three regions of interest are selected in each image for (1) signal-enhanced area (SI_{MEMRI}), (2) non-affine brain tissue (SI_{backgr}), and (3) background noise (SD_N). The expectable spatial signal enhancement quantified along the entirety of a single visual projection is presented in **Figure 3B**. Note the strong gradual increase of signal enhancement in retinal sections along the dorsoventral plane, which peaks at the optic nerve head. Additionally, note the lack of a relevant transsynaptic Mn^{2+} propagation into cortical layers under the applied experimental conditions (signal drop in the visual cortex). MIPs are highly illustrative to visualize the 3D positioning of the retino-tectal projection *in toto* (**Movie 1**). Accumulation of Mn^{2+} along the visual projection is determined by the kinetics of intracellular uptake into RGCs through voltage dependent Ca^{2+} channels and its fast axonal transport, as well as by the relatively low clearance from the target tissue[13]. According to our previous kinetic studies, Mn^{2+} dependent signal enhancement can be detected as early as 6 hr after injection. It further peaks at 24 hr and decreases back to baseline levels within 120 hr post-injection[9]. Therefore, to achieve optimum results, MEMRI should be performed 24 hr after injection, which represents half of the enhancement time required for rats[13].

Having outlined the principle for contrast enhancement of the visual projection by MEMRI, we further communicate the influences of two parameters – light condition and animal age – that may affect quantitative measurements:

(1) To test for stimulus-dependent accumulation of Mn^{2+} in midbrain centers, mice were kept either under light-stimulated conditions achieved by flashlight exposure of a defined frequency (5 Hz) and light intensity (3 W LED) or in complete darkness prior to the scan and during 24 hr of Mn^{2+} exposure. Quantitative analysis of the CNR 24 hr after *ivit* Mn^{2+} application reveals a significant increase in the signal intensity of dark-adapted retinae compared to light-stimulated conditions (66.29 ± 3.07 *vs.* 54.56 ± 3.08, $P \leq 0.05$, N = 7/8; **Figure 3C**). Given the gradient in signal enhancement between the peripheral retina and the optic nerve head (see **Figure 3B**), we assured to always analyze corresponding retinal sections within all experimental groups. Image analysis along the ventrodorsal plane revealed, as expected, that absolute CNR values are going down in both conditions. Importantly, the relative signal difference between dark and light adapted retinae remains persistent (data not shown). However, signal enhancement in the projection areas of LGN (26.97 ± 1.78 *vs.* 26.58 ± 1.05, $P = 0.9$, N = 7–2) and SC (25.09 ± 1.24 *vs.* 26.81 ± 1.55, $P = 0.4$, N = 7/8) is indistinguishable between light and dark conditioning environments (**Figure 3C**). This assay demonstrates that uptake of Mn^{2+} into retinal layers is sensitive to light exposure, whereas its propagation along the retino-tectal projection and accumulation in target areas is not influenced by coincident visual stimulation. Alternatively, the signal sensitivity of the 3 T scanner might be below the detection threshold for signal variation in the LGN or SC.

(2) To explore implications of the animal's age on MEMRI related signal enhancement of the visual projection, we analyzed mice between 3 and 26 months of age. CNR values in the LGN of 3 months old mice (23.49 ± 1.36, N = 12) do not differ from the signal intensity measured in mice aged 7 months (23.90 ± 0.81; $P = 0.79$, N = 16), 13 months (23.35 ± 1.29, $P = 0.94$, N = 10) or 26 months (25.10 ± 2.29, $P = 0.53$, N = 6; **Figure 3D**). Likewise, the signal intensity in the SC is unchanged between 3 months (19.01 ± 1.20) and 26 months of age (16.92 ± 2.18, $P = 0.37$; **Figure 3D**). Although a slight increase is evident in the CNR values of 26 month old retinae (38.49 ± 3.25), this increase does not reach significance when compared throughout all the groups ($P > 0.05$). These experiments indicate that signal enhancement in cerebral target areas of the visual projection is unaffected by visual stimulation and physiological aging.

Next, we demonstrate the sensitivity of MEMRI to detect structural alterations of the visual projection caused by acute and chronic axonopathy. To explore this, a model of Wallerian degeneration induced by traumatic ON injury[18] as well as an animal model displaying precocious, spontaneous degeneration of sensory projections including the visual pathway[19] were employed:

(1) Traumatic axonopathy induced by ON crush injury causes the breakage of axona fascicles. Consequently, retino-tectal transport of Mn^{2+} along the axonal cytoskeleton will be completely and sustainably blocked, as visualized by complete loss of Mn^{2+} enhanced signal in the LGN and SC analyzed one day (not shown), one week (**Figure 4A**, dotted lines), and 4 weeks (not shown) post injury. To clearly demonstrate the neuroanatomical and consecutive MR features of ON injury and to dissect them from the naïve state, the lesion was inflicted only unilaterally. This results in unaltered Mn^{2+} transport on the control side in contrast to tracer interruption on the side of the intervention. Analysis of CNR values in the deafferented areas confirms the complete absence of signal enhancement (not shown). This experiment further demonstrates that MEMRI is highly sensitive in detecting the location and severity of a lesion site by longitudinal assessment of the signal intensity along the projection before and after injury (**Figure 4B**). While the signal intensity along the ON before injury constantly stays above the background signal, there is a temporo-spatial drop in signal intensity to the background level one day after ON injury.

(2) Our earlier work demonstrated that Mn^{2+} dependent signal enhancement in the LGN is reduced in 10 months old mice lacking the NF-κB subunit p50 when measured 24 hr after injection[9]. Detecting this with a high consistence, we assumed an overall impairment in retino-tectal Mn^{2+} transport, possibly caused by reduced numbers of RGCs and related ON neuropathy in aging $p50^{KO}$ mice[19]. Alternatively, the reduced signal enhancement might be associated with a delayed neuronal uptake and propagation of Mn^{2+} from the vitreous body and along the pathological projection. The latter possibility can be explored by performing repetitive MR scans after a single application of 15 nmol Mn^{2+} and studying the kinetics of signal enhancement in the retina and LGN at early (8 and 24 hr) and late (48 and 72 hr) time points. In wild type and $p50^{KO}$ mice, retinal signal enhancement peaks at 8 hr at almost identical enhancement rates (43.52 ± 3.24 and 40.72 ± 2.79; $P = 0.6$, N = 3–6; **Figure 4C**, left). While signal enhancement remains high in wild types at 24 hr post injection, it declines in $p50^{KO}$ mice (43.38 ± 2.18 *vs.* 32.89 ± 1.54; $P \leq 0.01$, N = 5–8). During later phases (48 and 72 hr), signal enhancement decreases in both groups (with consistently lower CNR values in knock-out mice), thus excluding a delayed retinal Mn^{2+} uptake and propagation in $p50^{KO}$ mice. Corresponding results in the LGN of $p50^{KO}$ mice confirm this notion. Although the CNR is significantly lower between 8 and 48 hr post-injection ($P \leq 0.05$, N = 5–9), the kinetics of signal attenuation in $p50^{KO}$ mice corresponds to that in wild type mice (**Figure 4C**, right). Thus, the reduced temporo-spatial signal enhancement of the retino-tectal projection is due to reduced axon numbers originating from a limited RGC population rather than impaired transport kinetics. We propose MEMRI to be a valuable tool to screen genetic mouse mutants for projectional impairments in the CNS.
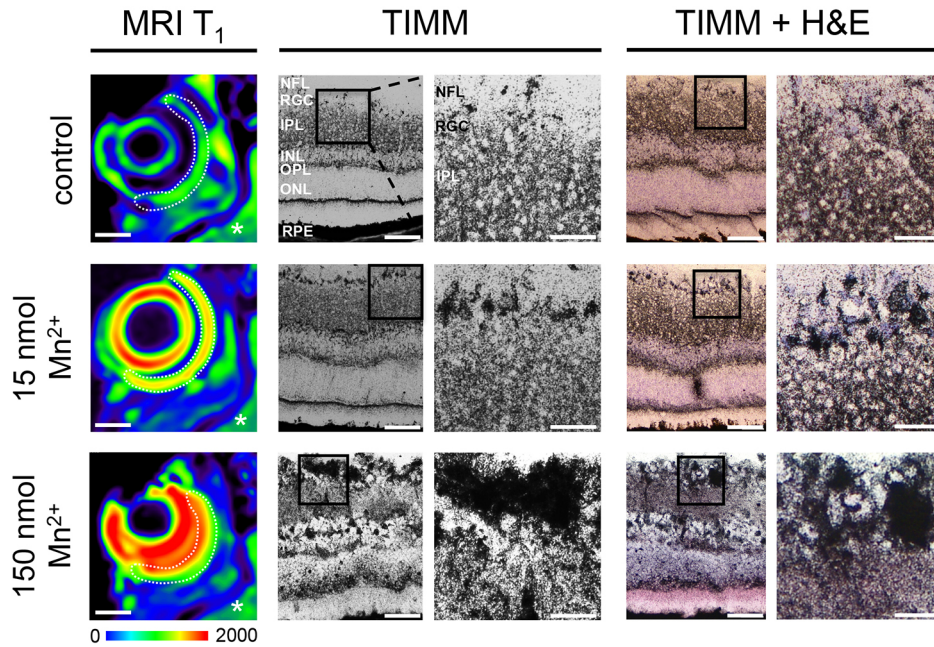
Figure 1. TIMM staining of Mn^{2+} uptake in RGCs. Representative heat-map images of T$_1$ weighted MRI (MRI T$_1$) show signal enhancement of the lens and the whole retinal circumference (dotted line) 24 hr after *ivit* application of 15 nmol, and hyper-intensive signal enhancement after application of 150 nmol Mn^{2+} (left). Warm colors represent higher signal values than cold colors. Scale bar: 1 mm. Middle/right: Mn^{2+} uptake by RGCs after *ivit* injection of MnCl$_2$ as detected by silver precipitation using TIMM staining (black color). PBS-treated control retina sections demonstrate rather weak staining and diffuse differentiation of the RGC layer (RGC) (top; N = 3). High magnification does not allow discrimination of individual cells (magnified insets). *Ivit* MnCl$_2$ application differentially increases overall silver staining across retinal layers, with a prominent silver precipitation particularly in the nerve fiber layer (NFL), RGC layer, and inner nuclear layer (INL; middle and bottom, magnified insets; N = 3). Colabeling of TIMM with H & E staining further confirms such layer specific Mn^{2+} accumulation (right panel). Scale bar, overview: 50 µm, magnification: 25 µm. IPL, inner plexiform layer; OPL, outer plexiform layer; ONL, outer nuclear layer; RPE, retinal pigment epithelium.
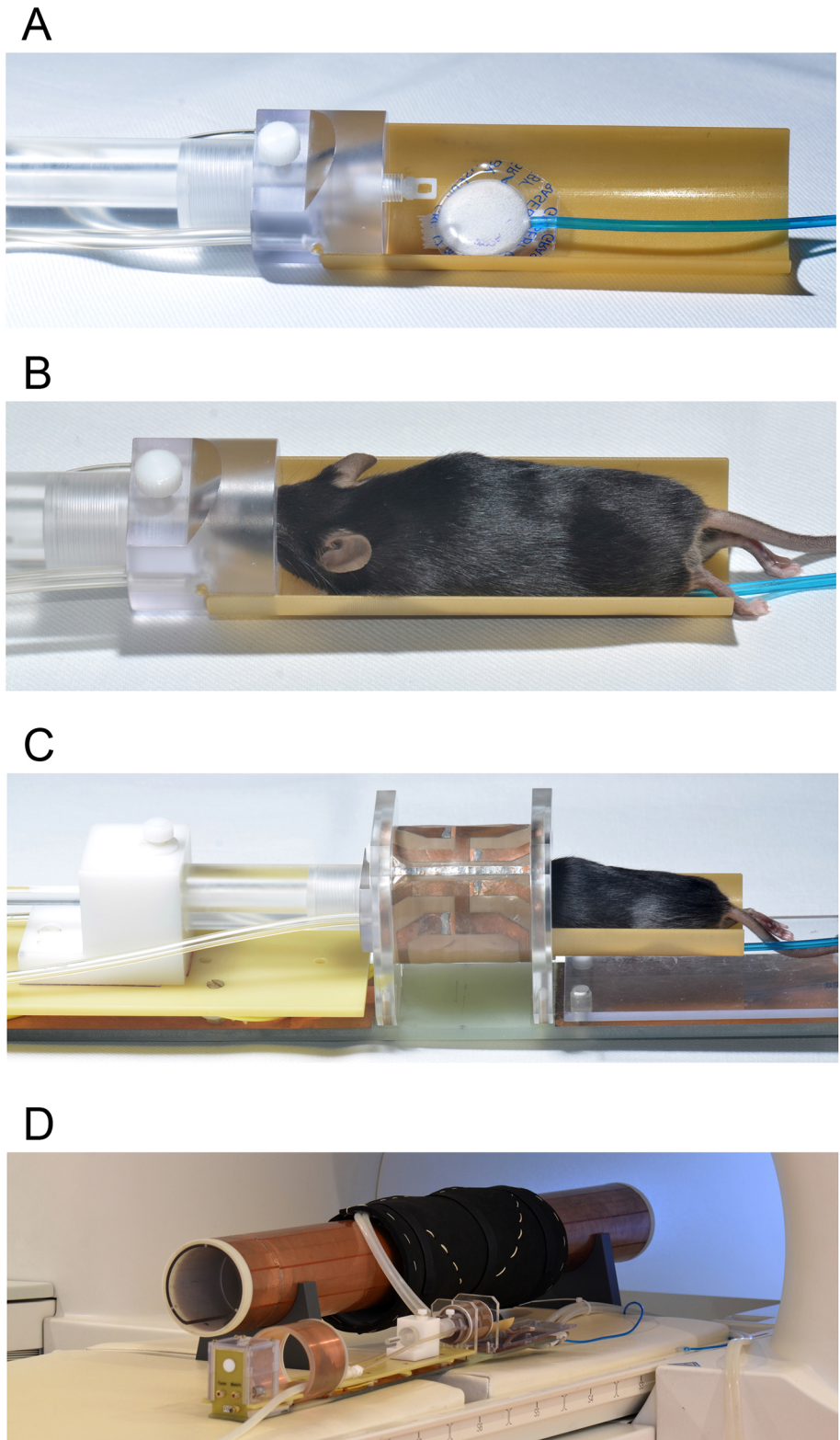
Figure 2. Photographs showing MRI equipment specifically for mouse MEMR image acquisition on a clinical 3T scanner. A) shows the custom-made mouse cradle with bite bar head fixation and the sensor for respiratory monitoring (white pad, blue tube). **B)** shows the positioned and fixed mouse in the cradle. The tubes to the left supply the anesthetic gas. **C)** exemplifies the positioning of the mouse head and cradle inside the linearly polarized Litz coil operating in transmit and receive mode. **D)** shows the coil platform in front of the shielding tube and the clinical 3 T scanner. The copper coated tube provides additional shielding from noise and blocks the MRI signal from the hot water based heating mat (black wrapping around the tube). **E)** visualizes the complete set-up of the animal coil within the pore of the 3 T scanner just prior to positioning the animal head precisely at the isocenter inside the scanner.
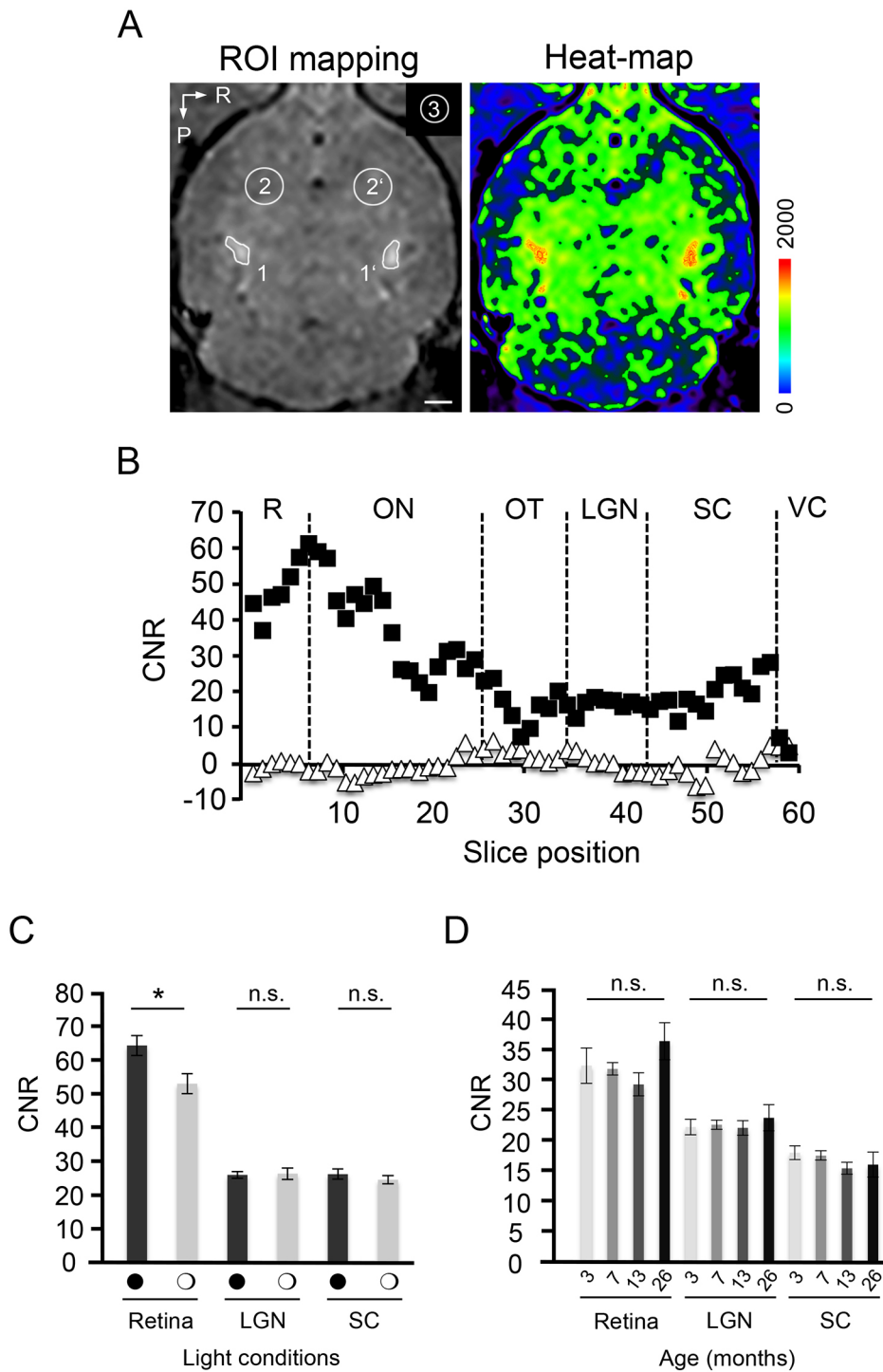
Figure 3. MEMRI of the naïve retino-tectal projection under various light and age conditions. A) Illustration of region of interest (ROI) mapping in enhanced LGN and background tissue on a transversal MRI recording (left). LGN specific signal enhancement is illustrated by heat map presentation (right). 1 and 1', left and right LGN; 2 and 2', background tissue; 3, noise; P, posterior; R, right. Scale bar: 100 µm. **B)** Spatial mapping of signal enhancement along a single retino-tectal projection as determined from originally acquired transversal MR image slices by MEMRI. Filled squares, Mn^{2+} dependent signal enhancement; open triangles, background signal. R, retina; ON, optic nerve; OT, optic tract; LGN, lateral geniculate nucleus; SC, superior colliculus; VC, visual cortex. Slice thickness, 200 µm. **C)** Light stimulation significantly reduces retinal signal enhancement. Enhancement in the LGN and SC is independent of visual stimulation. Filled circles, dark-adaptation; open circles, light adaptation. **D)** Signal enhancement is independent of increasing age between 3 and 26 months.
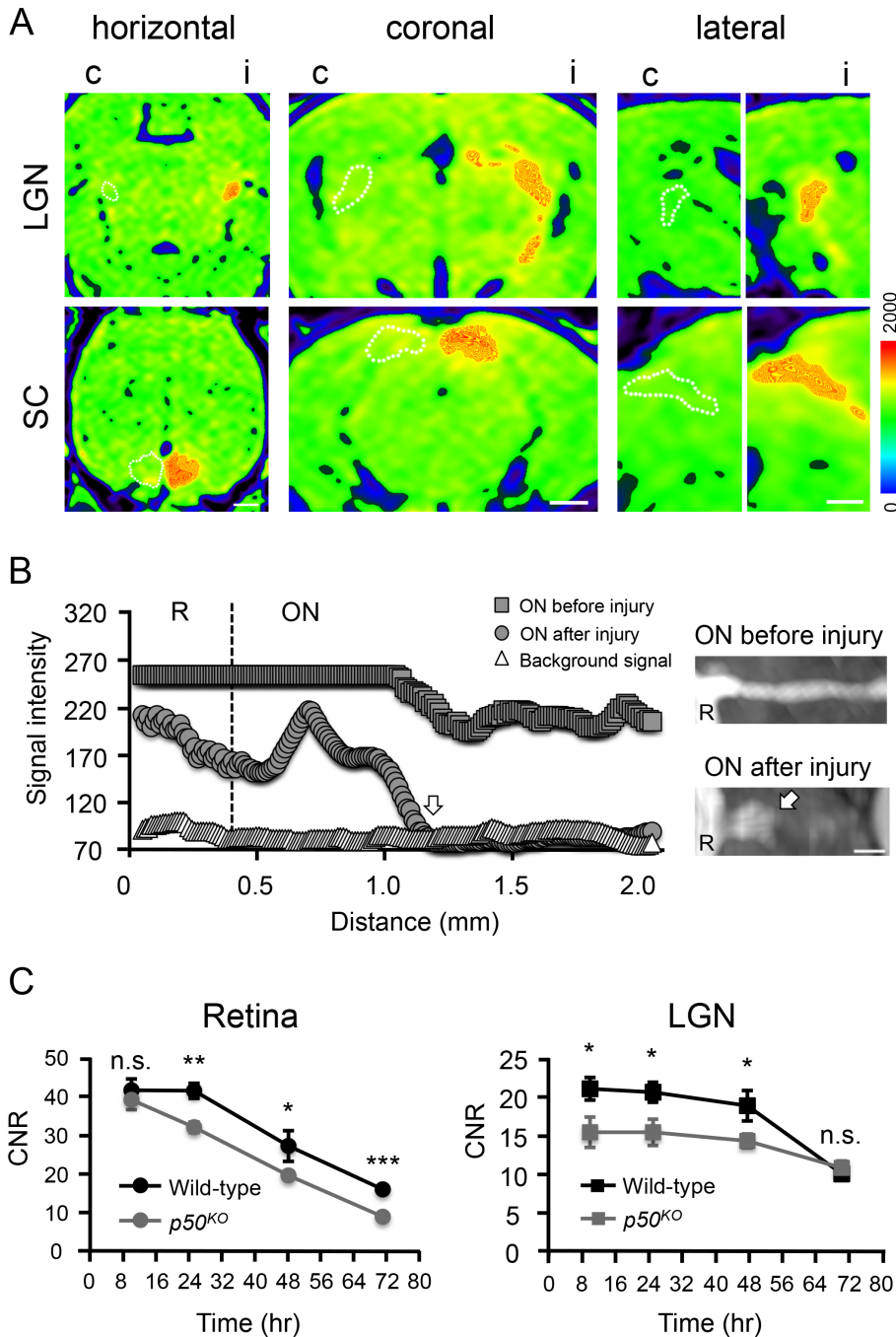
Figure 4. MEMRI of the retino-tectal projection under neurodegenerative conditions. A) MEMRI of bilaterally *ivit* injected mice performed one week after unilateral crush injury of the right ON. Multiplanar reconstructions of horizontal, coronal, and lateral views depict complete absence of signal enhancement in the LGN and SC for the injured hemisphere (dotted lines). c, contralateral hemisphere; i, ipsilateral hemisphere. Scale bar: 1 mm. **B)** MIP images and longitudinal MRI analysis of the spatial signal enhancement along the ON before and one day after injury. R, retina; ON, optic nerve; arrow, lesion site. Scale bar: 0.5 mm. **C)** Kinetics of signal enhancement under chronic neurodegeneration of the visual projection in *p50^KO* mice. Early (8 hr) uptake of Mn^{2+} into retinal cells is not affected, but is already reduced in the LGN of *p50^KO* mice. Repetitive MR imaging at 24, 48, and (only for retina) at 72 hr shows sustained signal reduction, but similar kinetics of Mn^{2+} transport and accumulation in the retina and LGN of *p50^KO* mice.

Movie 1: Animated, 3D heat-map presentation of the *in situ* contrast-enhanced retino-tectal projection. MR imaging was performed 24 hr after bilateral *ivit* injection of 15 nmol $MnCl_2$. Data are presented in the MIP mode. Slice thickness, 200 µm. Please click here to view this video.

Discussion

MEMRI of the visual system extends conventional neurobiological techniques for assessing functionality under naïve and pathological conditions. Apart from providing a unique insight into the integrity of an isolated CNS fiber tract, MEMRI can be easily supplemented with behavioral tests, e.g., optometry and visually based water tasks, to investigate the immediate consequences of a given paradigm for visual perception. It also links electrophysiological and histological investigations with functional visual characterization in vivo. The technique is highly reliable and reproducible with minor interindividual variances within identical groups (see error bars in **Figures 3, 4**). Intriguingly, at a dosage of 15 nmol, Mn^{2+} uptake and axonal transport are saturated processes, so that signal enhancement reaches a plateau which cannot be elevated by additional Mn^{2+} supply[9]. From a practical point of view, such a dose response characteristic minimizes, at least to some degree, injection associated variations in signal enhancement. Notably, the presented data on dosage and kinetics of Mn^{2+} signal enhancement are specific for mice and distinct from those in rats, which require an approximately 10-20x higher Mn^{2+} dosage and increased latency (36 hr) to achieve optimal contrast enhancement[13,23]. Additionally, enhancement along the visual projection remains consistent between an animal age of 3 and 26 months. This finding is in line with visual tests performed on aging mice and the fact that C57/B6 mice maintain normal visual activity up to 2 years of age[24]. Although we did not analyze individual mice longitudinally in the aging study, previous results clearly demonstrate the safety of repetitively administered Mn^{2+} dosages of 15 nmol for visual maintenance[9], which might be desired in longitudinal aging studies.

In accordance with the notion that Mn^{2+} is incorporated into RGCs, we show Mn^{2+} uptake into their somata by TIMM staining which relies on silver precipitation of free metal ions, as applied by Angenstein et al. for intracerebral Mn^{2+} detection following its systemic application[22]. Previously, intracerebral Mn^{2+} distribution was detected by autoradiography of $^{54}Mn^{2+}$ isotope to delineate neuronal circuits of the rat CNS[25], but not at the cellular level. Here, TIMM staining allows the attribution of Mn^{2+} uptake to distinct cell populations within the exposed retina, where we find prominent silver precipitation in the RGC and nerve fiber layers. It should be noted that the protocol applied shows improved detection by TIMM staining after application of a dosage of 150 nmol compared to 15 nmol Mn^{2+}. Although Mn^{2+} uptake and its axonal transport are already saturated at 15 nmol, thus, conferring no additional CNR increase along the retino-tectal projection at higher dosages, excessive supplementation might increase the availability of free, protein unbound Mn^{2+} and thus render it accessible for silver precipitation. Future refinements in staining sensitivity will allow the correlation of MEMRI-based CNR values of specific CNS projections with the cellular location of Mn^{2+} enrichment within a defined histological region. Such a capability might also be useful for the characterization and quantification of Mn^{2+} distribution in other CNS regions outside the visual projection. Likewise, Mn^{2+} has been employed in a kainate toxicity model to visualize degeneration and regeneration of hippocampal mossy fibers[26].

Mn^{2+} is taken up by voltage dependent calcium channels and is intracellularly distributed by active axonal transport, which can be blocked by colchicine treatment[25,27]. Visual stimulation experiments on rats receiving an intraperitoneal dosage of $MnCl_2$ have revealed an increased signal enhancement in the inner and, in particular, outer retina[28]. Thereby, dark adaptation further raises signal intensities in the outer retinal layers compared to rats exposed to room light conditions only, thus indicating sensitivity of retinal Mn^{2+} uptake to visual stimulation[28]. Similarly, we find enhanced signal intensity in the retina of dark adapted mice compared to mice exposed to visual stimulation after ivit Mn^{2+} application. This might be related to the specific electrophysiological properties of the retina and the generation of a continuous dark current in photoreceptor cells. Since Ca^{2+} influx into outer segments of photoreceptors significantly contributes to the constitution of the dark current, their generation might be accompanied by enhanced co-uptake of Mn^{2+} into the photoreceptor cell layer under darkness. In contrast, light stimulation reduces the dark current and causes hyperpolarization of photoreceptor cells[29]. Thereby, overall Mn^{2+} uptake might be diminished under light conditions.

For reliable usage of MEMRI, it is important to clarify whether the more pronounced Mn^{2+} uptake into the dark-adapted retina alters signal enhancement along other parts of the visual projection or even its entire extension. Stimulation-dependent changes in MEMRI signal intensity of cerebral networks have been demonstrated for the acoustic system after intraperitoneal Mn^{2+} application[30]. In this study by Yu et al., rats were exposed to variable noise frequencies before the MR scans and T_1 weighted signal enhancement of the inferior colliculi was subsequently investigated. Acoustic stimulation was found to significantly increase MEMRI signal intensities in a tonotopic representation, thus exemplifying the fMRI-like character of activity-dependent Mn^{2+} accumulation[30]. In contrast, in our experimental set up Mn^{2+} accumulation in the LGN and SC appears independent of visual stimulation. However, such differences in sensory brain mapping attempts might arise from the lower magnetic field and limited threshold of detection of our 3 T scanner in comparison to the high field 7 T scanner used by Yu et al[30].

To date, it is not known to what extent biophysical parameters affect anterograde axonal transport of Mn^{2+} and how MEMRI might serve as an indicator for electrical activity. Nevertheless, it appears that Mn^{2+} transmission by RGCs occurs, at least in part, independently of light specific stimulation and electrical input received from bipolar cells. Alternatively, the net effect of electrical activity within the retino-tectal projection might be a result of electrical stimulation of dark-responsive 'OFF-RGCs' and light-responsive 'ON-RGCs'. Such an interpretation is supported by the finding that Mn^{2+} transport along the retino-tectal projection is not impaired in mouse strains with poor vision, such as CBA mice that carry the rd1 mutation of the Pde6b gene causing retinal degeneration[11]. In a kinetic study on wild type sighted and CBA mice, comparable transportation rates were observed during the initial influx phase (at 2.5 hr post-injection) and for the final signal enhancement (at 24 hr) in the LGN and SC[11].

Taken together, these observations support the notion that MEMRI, e.g., of the visual system as exemplified here, represents a valuable measure for structural integrity and metabolic stability rather than for electrical activity. Practically, the seemingly stable independence of signal enhancement in cerebral LGN and SC from light exposure allows for robust handling and housing of animals without special care concerning illumination. On the other hand, for MEMRI studies that focus on retinal signal enhancement, it is necessary to keep animals under tightly controlled light conditions prior to the scan.

Among the physiological parameters that affect Mn^{2+} axonal transport rates and subsequent MEMRI signal enhancement, stability of body temperature might be of particular importance. This is indicated by studies on intranasal Mn^{2+} for enhancement of primary olfactory projection targets in the brain, where enrichment was found to be significantly diminished at a temporary reduction of body temperature to 30 °C compared to signal enhancement under normal body temperature[27]. Therefore, body temperature should be monitored and adjusted prior to and during the MR scans not only to protect the animals' health, but also to normalize physiological parameters of Mn^{2+} propagation.

Since pathophysiological alterations and metabolic impairments affect the axonal transport efficacy of Mn^{2+}, signal enhancement in projection centers, *e.g.*, LGN and SC, can serve as a measure for the structural integrity and functional activity of this pathway. Here, we present two different conditions of ON degeneration and illustrate that Mn^{2+} propagation and enrichment in thalamic and midbrain centers varies as a function of axonal integrity. Acute ON injury results in a total signal loss immediately after injury, which does not recover within 4 weeks due to the lack of relevant axonal regeneration, whilst slow axonal degeneration in the *p50*^{KO} mutant is reflected by reduced CNR values in the LGN. Given the possibility of longitudinal imaging, this application of MEMRI might be valuable for monitoring postlesional growth responses of the ON and allow for the investigation of proregenerative genetic or pharmacological interventions to RGCs.

Additionally, we present MEMRI as a highly sensitive method to detect gradual impairments in signal enhancement that are associated with chronic axonal degeneration processes. The transcription factor NF-κB is involved in neuronal maintenance and mice with deletion of the p50 subunit of NF-κB display age-dependent neuronal cell loss and axonal degeneration within the visual system[19]. In addition to histological and electron microscopic analyses, MEMRI of the retino-tectal projection is able to identify phenotypic alterations in these mice. By acquisition of serial T_1 weighted MR images following *ivit* Mn^{2+} application, we distinguished an overall reduced from a simply delayed Mn^{2+} transport along the visual pathway in these *p50*^{KO} mice. Thereby, repetitive data acquisition by MEMRI after a single Mn^{2+} application enables the definition of axonal transport kinetics and neurophysiological alterations in the invaluable pool of available genetically modified mice. Currently, several modifications of MEMRI are under investigation aiming to make this technique safe for diagnostic applications in humans. A promising approach of high clinical relevance, which constitutes an alternative to *ivit* injection, is the delivery of Mn^{2+} as eye drops. Thereby, topical administration of 1 M $MnCl_2$ yielded a significant signal enhancement by 20% in the SC when images were acquired on a 4.7 T animal scanner[31]. The method was able to detect extensive ON degeneration following retinal ischemia[31], and the concentration applied proved safe when repetitively applied in monthly intervals[32]. Given the relatively high neurotoxicity of Mn^{2+}[9], future studies are required to define if this strategy is sensitive enough to detect ON pathologies already in early states when applied in tolerable concentrations. Such research will be useful to support clinically relevant MEMRI applications, *e.g.*, for the diagnosis of multiple sclerosis and other neuropathies.

In summary, our study demonstrates that MEMRI is a powerful experimental approach to study retino-tectal circuitries in mice, thus extending optometric tasks for assessing the functionality of the visual system.

Disclosures

The authors declare that they have no competing financial interests.

Acknowledgements

References

1. Kretz, A. *et al*. Simvastatin promotes heat shock protein 27 expression and Akt activation in the rat retina and protects axotomized retinal ganglion cells in vivo. *Neurobiol Dis.* **21**, 421-430 (2006).
2. Lima, S. *et al*. Combinatorial therapy stimulates long-distance regeneration, target reinnervation, and partial recovery of vision after optic nerve injury in mice. *Int Rev Neurobiol.* **106**, 153-172 (2012).
3. Lima, S. *et al*. Full-length axon regeneration in the adult mouse optic nerve and partial recovery of simple visual behaviors. *Proc Natl Acad Sci U S A.* **109**, 9149-9154 (2012).
4. Goetze, B. *et al*. Vision and visual cortical maps in mice with a photoreceptor synaptopathy: reduced but robust visual capabilities in the absence of synaptic ribbons. *Neuroimage.* **49**, 1622-1631 (2010).
5. Luo, X. *et al*. Three-dimensional evaluation of retinal ganglion cell axon regeneration and pathfinding in whole mouse tissue after injury. *Exp Neurol.* **247**, 653-662 (2013).
6. Pautler, R. G. *et al*. *In vivo* neuronal tract tracing using manganese-enhanced magnetic resonance imaging. *Magn Reson Med.* **40**, 740-748 (1998).
7. Watanabe, T. *et al*. Mapping of retinal projections in the living rat using high-resolution 3D gradient-echo MRI with Mn^{2+}-induced contrast. *Magn Reson Med.* **46**, 424-429 (2001).
8. Pautler, R. G. *In vivo*, trans-synaptic tract-tracing utilizing manganese-enhanced magnetic resonance imaging (MEMRI). *NMR biomed.* **17**, 595-601 (2004).
9. Haenold, R. *et al*. Magnetic resonance imaging of the mouse visual pathway for *in vivo* studies of degeneration and regeneration in the CNS. *Neuroimage.* **59**, 363-376 (2012).
10. Lindsey, J. D. *et al*. Magnetic resonance imaging of the visual system *in vivo*: transsynaptic illumination of V1 and V2 visual cortex. *Neuroimage.* **34**, 1619-1626 (2007).
11. Bearer, E. L. *et al*. Role of neuronal activity and kinesin on tract tracing by manganese-enhanced MRI (MEMRI). *Neuroimage.* **37 Suppl 1**, S37-46 (2007).
12. Mendonca-Dias, M. H. *et al*. Paramagnetic contrast agents in nuclear magnetic resonance medical imaging. *Semin Nucl Med.* **13**, 364-376 (1983).
13. Thuen, M.*, et al*. Manganese-enhanced MRI of the optic visual pathway and optic nerve injury in adult rats. *J Magn Reson Imaging.* **22**, 492-500 (2005).
14. Sandvig, I. *et al*. *In vivo* MRI of olfactory ensheathing cell grafts and regenerating axons in transplant mediated repair of the adult rat optic nerve. *NMR biomed.* **25**, 620-631 (2012).

15. Chan, K. C. *et al. In vivo* retinotopic mapping of superior colliculus using manganese-enhanced magnetic resonance imaging. *Neuroimage.* **54**, 389-395 (2011).
16. Chan, K. C. *et al. In vivo* chromium-enhanced MRI of the retina. *Magn Reson Med.* **68**, 1202-1210 (2012).
17. Herrmann, K. H. *et al.* Possibilities and limitations for high resolution small animal MRI on a clinical whole-body 3T scanner. *Magma.* **25**, 233-244 (2012).
18. Villegas-Perez, M. P. *et al.* Rapid and protracted phases of retinal ganglion cell loss follow axotomy in the optic nerve of adult rats. *J Neurobiol.* **24**, 23-36 (1993).
19. Takahashi, Y. *et al.* Development of spontaneous optic neuropathy in NF-κB50-deficient mice: requirement for NF-κBp50 in ganglion cell survival. *Neuropathol Appl Neurobiol.* **33**, 692-705 (2007).
20. Herrmann, K. H. P. *et al.* MRI compatible small animal monitoring and triggering system for whole body scanners. *Z Med Phys.* **24**, 55-64 (2013).
21. Danscher, G., & Zimmer, J. An improved Timm sulphide silver method for light and electron microscopic localization of heavy metals in biological tissues. *Histochemistry.* **55**, 27-40 (1978).
22. Angenstein, F. *et al.* Manganese-enhanced MRI reveals structural and functional changes in the cortex of Bassoon mutant mice. *Cereb cortex.* **17**, 28-36 (2007).
23. Thuen, M. *et al.* Manganese-enhanced MRI of the rat visual pathway: acute neural toxicity, contrast enhancement, axon resolution, axonal transport, and clearance of Mn(2+). *J Magn Reson Imaging.* **28**, 855-865 (2008).
24. Lehmann, K. *et al.* Vision and visual plasticity in ageing mice. *Restor Neurol Neurosci.* **30**, 161-178 (2012).
25. Takeda, A. *et al.* Manganese transport in the neural circuit of rat CNS. *Brain Res Bull.* **45**, 149-152 (1998).
26. Nairismagi, J. *et al.* Manganese-enhanced magnetic resonance imaging of mossy fiber plasticity *in vivo*. *Neuroimage.* **30**, 130-135 (2006).
27. Smith, K. D. *et al. In vivo* axonal transport rates decrease in a mouse model of Alzheimer's disease. *Neuroimage.* **35**, 1401-1408 (2007).
28. Berkowitz, B. A. *et al.* Noninvasive and simultaneous imaging of layer-specific retinal functional adaptation by manganese-enhanced MRI. *Invest Ophthalmol Vis Sci.* **47**, 2668-2674 (2006).
29. Schnapf, J. L. B. D.A. How photoreceptor cells respond to light. *Sci. Am.* **256**, 8 (1987).
30. Yu, X. *et al. In vivo* auditory brain mapping in mice with Mn-enhanced MRI. *Nat Neurosci.* **8**, 961-968 (2005).
31. Sun, S.W. *et al.* Noninvasive topical loading for manganese-enhanced MRI of the mouse visual system. *Invest Ophthalmol Vis Sci.* **52**, 3914-3920 (2011).
32. Sun, S.W. *et al.* Impact of repeated topical-loaded manganese-enhanced MRI on the mouse visual system. *Invest Ophthalmol Vis Sci.* **53**, 4699-4709 (2012).